Static and seismic response analyses of new seismic integrated ceiling using FEM

Zhilun Lyu[*1], Masakazu Sakaguchi[2], Tomoharu Saruwatari[3] and Yasuyuki Nagano[**4]

[1]Okuju Corporation, 5-3-7 Nishitemma, Kita-Ku 530-0047, Osaka, Japan
[2]Asahibuilt Industry, Corporation Limited, 4-32-8, Kamatahommachi, Otaku 144-0052, Tokyo, Japan
[3]JSOL Corporation, 2-2-4 Tosabori, Nishi-Ku 550-0001, Osaka, Japan
*[4]Graduate School of Information Science, University of Hyogo, 7-1-28, Minatojima-minamimachi,
Chuo-Ku 650-0047, Kobe, Japan*

Abstract. The seismic performances of suspended ceilings are mostly evaluated via shaking table tests, whose results can be intuitively understood. However, these tests become impracticable when the ceiling surface area is beyond the limit of the shake table. Hence, simulation analysis becomes an alternative method. However, simulation analysis for suspended ceilings has not been yet developed and is used as an auxiliary method. To provide a new approach for evaluating the seismic performances of suspended ceilings, we have proposed numerical models for a new seismic integrated ceiling in previous studies, including 1) models (shell elements) for the intersections of the ceiling members and 2) models (beam elements) for ceiling units. Based on our previous studies, we created a model with a ceiling surface area of 264 m^2 and analyzed via LS-DYNA as an example to evaluate the seismic performance of the new seismic integrated ceiling. To confirm the seismic behavior of the new seismic integrated ceiling during earthquakes, as an example, JMA Kobe earthquake waves were input into the simulation model for the first time. Via the simulation analysis, it was confirmed that the seismic performance of the new seismic integrated ceiling was satisfactory even when the ceiling surface area exceeded 200 m^2.

Keywords: integrated ceiling; numerical model; seismic ceiling; seismic evaluation; simulation analysis; suspended ceiling;

1. Introduction

1.1 Types of suspended ceilings

Suspended ceilings have been widely used as the interior in almost all constructions around us, including but not limited to office buildings, railway platforms and underground shopping malls.

The suspended ceilings can be roughly categorized into two types according to the installation methods of the ceiling boards and types of components: the one in which ceiling boards are firmly connected to the ceiling members via screws, and the other in which ceiling boards are placed

---

above the grid of the ceiling members as shown in Fig. 1. In this paper, the former is called "conventional suspended ceilings", the latter called "integrated ceilings", irrespective of all the other details. Both conventional suspended ceilings and integrated ceilings are widely used in Japan.

Table 1 compares conventional suspended ceilings and integrated ceilings in Japan based on their functionality and workability in the installation and maintenance of embedded equipment such as lighting and aircon systems, their seismic resistance, seismic requirements, and difficulty to meet the seismic requirements of 2.2 G which is required in the Notification no.771 (2013) of the Ministry of Land, Infrastructure, Transportation, and Tourism, Japan (hereinafter, refer to as the Notification no. 771). It shows that integrated ceilings have the advantages of "easier construction workability", "better functionality" and "easier maintenance" than conventional ceilings, but they have the disadvantage of being inferior in earthquake resistance. Therefore, improvement of seismic performance such as weight saving of the ceiling components of integrated ceiling system is important to disseminate this system.

1.2 Existing studies

The existing studies on the seismic performances of suspended ceilings mainly rely on shaking table tests. For instance, Ryu *et al*. (2017), Lu *et al*. (2018), and Sasaki *et al*. (2017) used shake tables to examine the seismic performances of suspended ceilings with large areas; Fiorino *et al*. (2019) conducted shaking table tests to evaluate the seismic performances of specimens made of indoor partition walls, outdoor facade walls, and suspended continuous ceilings; Qi *et al*. (2020) conducted a series of shaking table tests to investigate the vibration properties of suspended ceilings while considering their interactions with the surrounding equipment; Pourali *et al*. (2018) examined the seismic compatibility of low-damage drywall partitions and suspended ceilings by shaking table tests; Soroushian *et al*. (2019) conducted a series of full-scale system-level experiments to clarify the response of the integrated ceiling-piping-partition systems.

Simulation analysis, however, is a preliminary manner and is used as an auxiliary measure. For example, Gilani *et al*. (2017) modeled and evaluated the seismic performance of the conventional suspended ceilings without bracings. The details of the simulation models, e.g., cross-sections of ceiling members, the modeling of intersections of ceiling members etc., are not clear.

Isobe *et al*. (2017) proposed a new method to model and evaluate suspended ceilings in school gymnasiums (conventional suspended ceilings with slope) using the ASI-Gauss code. Although the mechanism of collapse could be confirmed by the numerical model, damage occurred in different parts compared with the shaking table tests. Moreover, the failure conditions for the metal fittings were simply set as follows: the metal fittings failed when forces reach the predefined values.

Concerning integrated ceilings, Kambe *et al*. (2017) used a multi-degree-of-freedom model to discuss the effect of the numbers of bracings on the seismic performance of the integrated ceilings. Though seismic waves have been input, all of which are input in only one direction, separately. Moreover, the simulation analysis discussed the effect of the number of bracings in per unit on the seismic performance in the ceiling unit level, but not in actual sizes.

Conversely, studies on structural members frequently use the finite element method (FEM) to confirm the seismic performance of the structural members. Mizushima *et al*. (2018) created a detailed finite element (FE) model using the LS-DYNA software. Their paper shows that the behaviors of structural members can be analytically simulated with extremely high accuracy. In
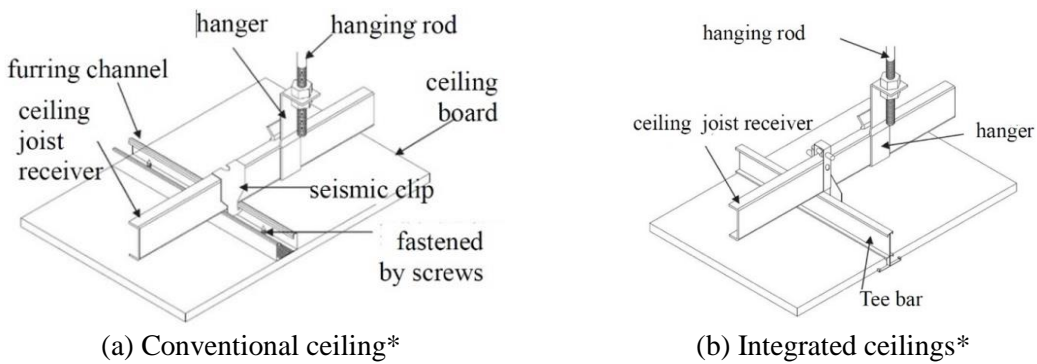
(a) Conventional ceiling*   (b) Integrated ceilings*

Fig. 1 Types of suspended ceilings (examples)

* Based on Guidelines for safety measures against accidental fall of ceilings and other non-structural components (2015.1.20. p191)

Table 1 Difference of conventional suspended ceilings and integrated ceilings (general)

	Conventional suspended ceilings	Integrated ceilings (general)
Functionality (Flexibility)	Not good	good
Maintenance of embedded equipment	Not easy	easy
Construction workability	Not good	good
Seismic resistance (in-plane rigidity)	high	low
Difficulty to meet the seismic requirements of 2.2 G	Easy to meet	Difficult to meet

* Specification proposed by the Rock Wool Association

addition, Ushio *et al*. (2019) proposed a new design method to improve the seismic performance of the tower cranes with the LS-DYNA. Hence, it is believed that the seismic performance of the suspended ceilings can be evaluated by using FEM.

1.3 Purposes

One of our authors developed a new type of seismic integrated ceiling (hereinafter, referred to as the new seismic integrated ceiling) using ceiling members with completely different cross sections (Fig. 4 in the section 2.1 and Fig. 6 in the section 2.3). Thereby, screws were used to connect the ceiling members at junctions. Based on static tests, we have proposed a new approach, which the screw joints between main bars (or W bars) and cross bars are called rotation springs (Lyu *et al*. 2019), to evaluate the new seismic integrated ceiling at the unit level (18 m^2) using LS-DYNA. The seismic performance of the new seismic integrated ceiling under 2.2 G has been proved by static tests and simulation analysis at the ceiling unit level according to the current standards in Japan. It is also proved that the numerical model can reproduce the static tests and thus can used to evaluate the seismic performance of the new seismic integrated ceiling. Since then, the new seismic integrated ceilings have been installed in 7 facilities, all of which have area beyond 200 m^2. However, the seismic performances of real-sized seismic integrated ceilings (e.g., ceilings with area over 200 m^2, i.e., the least area of ceiling surface for specific ceilings) under
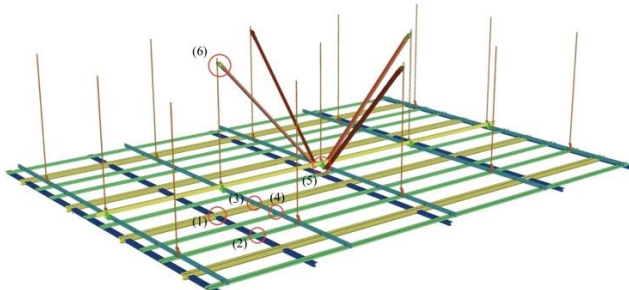
Fig. 2 Overview of new seismic integrated ceiling (example)

(a) main bar - cross bar

(b) W bar - cross bar

(c) main bar - ceiling joist receiver

(d) W bar - ceiling joist receiver
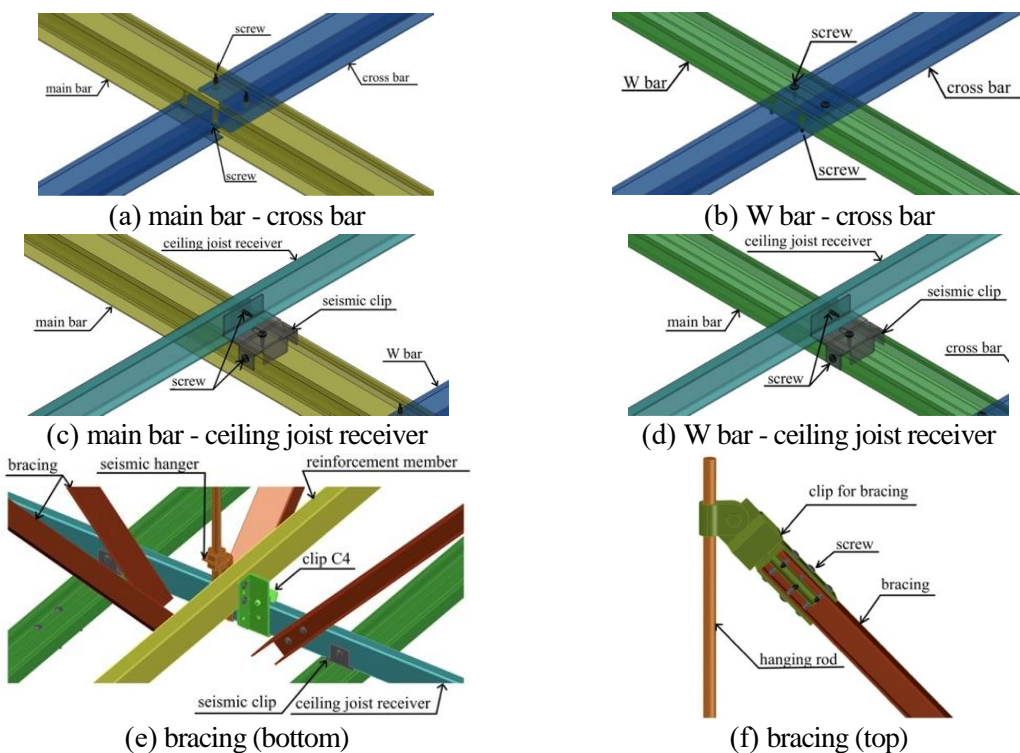
(e) bracing (bottom)

(f) bracing (top)

Fig. 3 Junctions

recorded earthquake waves are not clear, as the tests in real-sized level are not required by the current standards.

This study aims to use static analysis to evaluate the seismic performances of new seismic integrated ceilings with large areas. To provide the possibilities of simulation analysis under recorded earthquake waves, JMA Kobe earthquake waves were input into simulation models as an example. A simulation model with ceiling surface area of 264 m^2 is discussed as an example. Large area refers to areas over 200 m^2, which although is the least area for suspended ceilings according to Notification no.771.

In our previous studies, the seismic performances of suspended ceilings were evaluated at the ceiling unit level by both static tests and simulation analysis. However, the behaviors of suspended
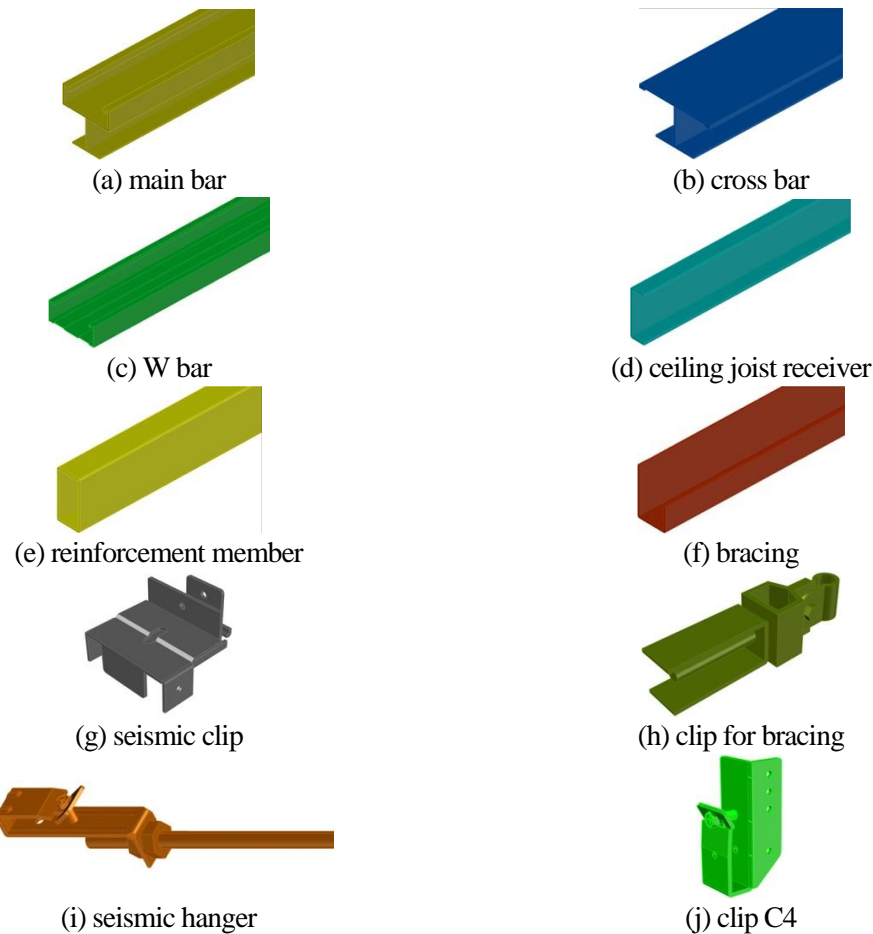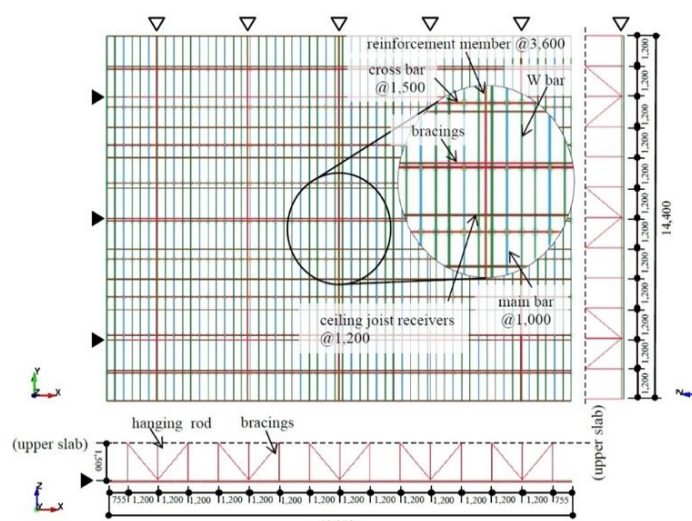
(a) main bar

(b) cross bar

(c) W bar

(d) ceiling joist receiver

(e) reinforcement member

(f) bracing

(g) seismic clip

(h) clip for bracing

(i) seismic hanger

(j) clip C4

Fig. 4 Ceiling members and metal fittings

Fig. 5 Overview of the numerical model (unit: mm)

(a) main bar   (b) cross bar   (c) W bar

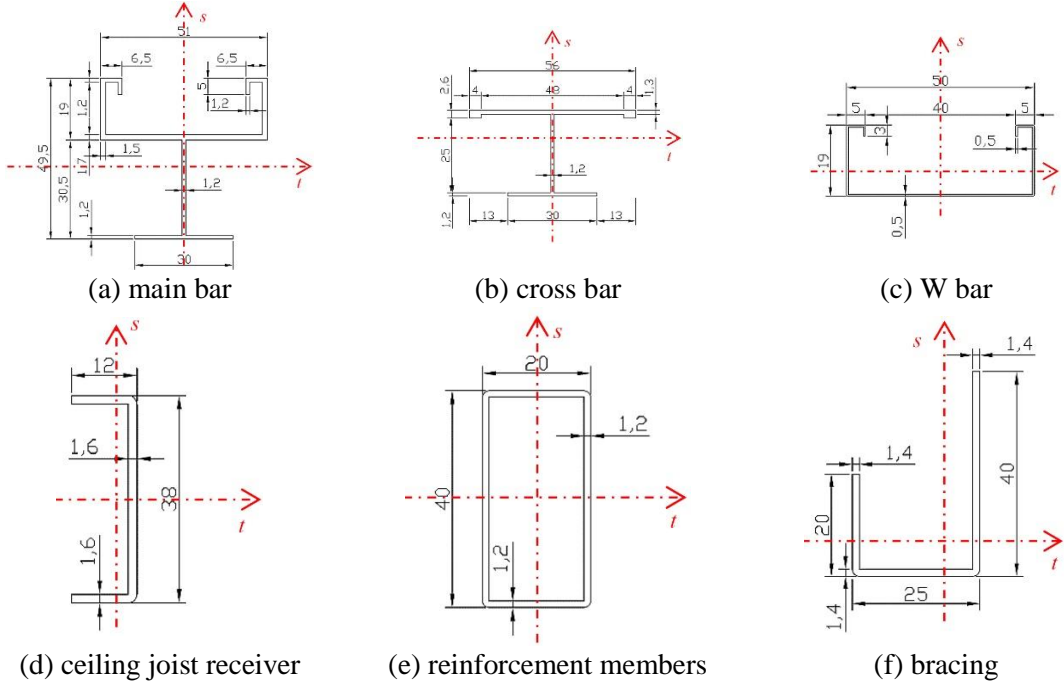(d) ceiling joist receiver   (e) reinforcement members   (f) bracing

Fig. 6 Cross sections of ceiling members

ceilings vary as the placement of ceiling members and size of ceiling surface area change. Therefore, it is always preferable to evaluate the seismic performances of real-sized suspended ceilings than to evaluate the performances of impractically small ceilings. In most cases, suspended ceilings cannot be evaluated in their actual sizes by shaking table tests because of the size limitation of shaking table. On the other hand, since evaluation by a simulation analysis using supercomputer has nothing with the size of the ceiling. Thus, simulation analysis should be suitable to evaluate the seismic performances of the suspended ceilings with large area.

2. Numerical model

2.1 Construction system of new seismic integrated ceiling

Fig. 2 depicts an example of the new seismic integrated ceilings in 3D CAD. The junctions and ceiling members (including metal fittings) used in the new seismic integrated ceilings are shown in Fig. 3 and Fig. 4, respectively. Colors in Figs. 2-4 are only used to distinguish different ceiling members. Details of sections and sizes of main bar, cross bar, W bar, ceiling joist receiver, reinforcement member and bracing, which related to the numerical models, are given in the Section 2.3.

The new seismic integrated ceiling consists of extruded aluminum profiles, steel profiles, seismic metal fittings and glass wool panels. Following is the summary of ceiling members and metal fittings used in the new seismic integrated ceiling. Because this paper focuses on the main structure, effects of the surrounding walls and glass wool panels are not considered. Thus, moldings and glass wool panels are omitted in this paper, including Figs 2-4.

Table 2 Cross-sectional properties of each ceiling member

Ceiling members (dimension)	Cross-sectional area (mm^2)	Second moment of area Itt (mm^4)	Second moment of area Iss (mm^4)
Main bars (Fig. 6(a))	230	53,931[*]	62,375[*]
Cross bars (Fig. 6(b))	150	21,417[*]	28,773[*]
W bars (C-50 × 19 × 0.5)	51	2,700	19,900
Ceiling joist receivers (C-38 × 12 × 1.6)	94	1,830	1,100
Reinforcement members (□-40 × 20 × 1.2)	134.5	27,300	9,230
Bracings (L-40 × 25 × 20 × 1.4)	114.2	16,055	12,038
Hanging rods (W3/8)	49.1	191	191

[*] Calculated values according to the cross section

Table 3 Physical properties of each ceiling member

Ceiling members (mark of material)	Mass-density (ton/mm^3)	Young's modulus (N/mm^2)	Poisson's ratio	Yield stress (N/mm^2)
Main bars (A6063SS-T5)	2.70×10^{-9}	7.0×10^4	0.33	145
Cross bars (A6063SS-T5)	2.70×10^{-9}	7.0×10^4	0.33	145
W bars (SGCC)	7.86×10^{-9}	2.05×10^5	0.30	205
Ceiling joist receivers (SGCC)	7.86×10^{-9}	2.05×10^5	0.30	205
Hanging rods (SGCC)	7.86×10^{-9}	2.05×10^5	0.30	205
Bracings (SGCC)	7.86×10^{-9}	2.05×10^5	0.30	205
Reinforcement members (STKMR11A)	7.85×10^{-9}	2.05×10^5	0.30	203

(a) main bar (the list numbers are in accordance with Fig. 4)

Extruded aluminum profile. Main bar is the main substrate member which composes the ceiling surface. Grooves are used to lay glass wool panels.

(b) cross bar

Extruded aluminum profile. Cross bar is allocated perpendicularly to the main bar. Grooves are used to lay glass wool panels.

(c) W bar

Steel profiles, which is allocated paralleled to the main bar.

(d) ceiling joist receiver

C-shaped ceiling member which connects main bar and W bar.
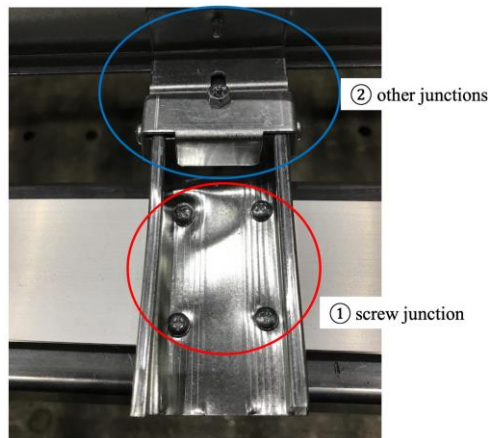
(e) reinforcement member

Fig. 7 Junctions of ceiling members

(a) main bar × cross bar   (b) W bar × cross bar
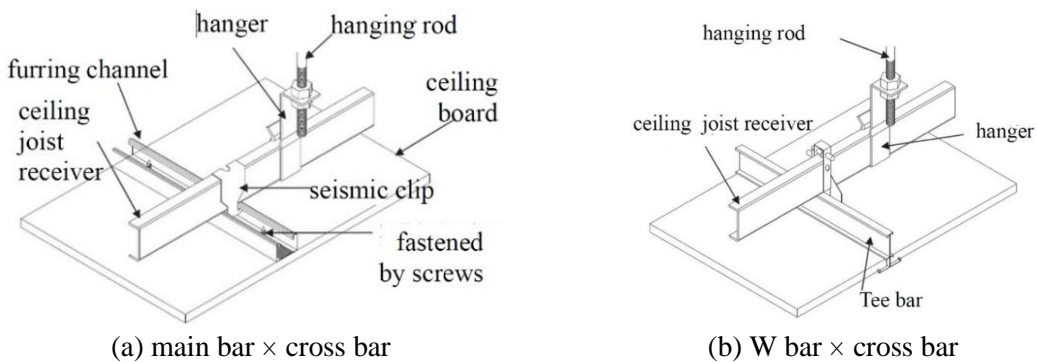
Fig. 8 Rigidities of the rotation springs

Square-shaped member which used to connect bracing.

(f) bracing

U shaped member which connects hanging rod in seismic hanger and ceiling joist receiver (or reinforcement member).

(g) seismic clip

A kind of metal fitting which connects main bar (or W bar) and ceiling joist receiver. It is designed to resist harder earthquakes and vibrations.

(h) clip for bracing

A kind of metal fitting which used to connect the bracing and hanging rod at the top part of bracing.

(i) seismic hangers

A kind of metal fitting with a screw which connects ceiling joist receiver and upper slab.

(j) clip C4

A kind of metal fitting which connects the ceiling joist receiver and the reinforcement member. C4 is the product name originated from the manufacture.

* moldings

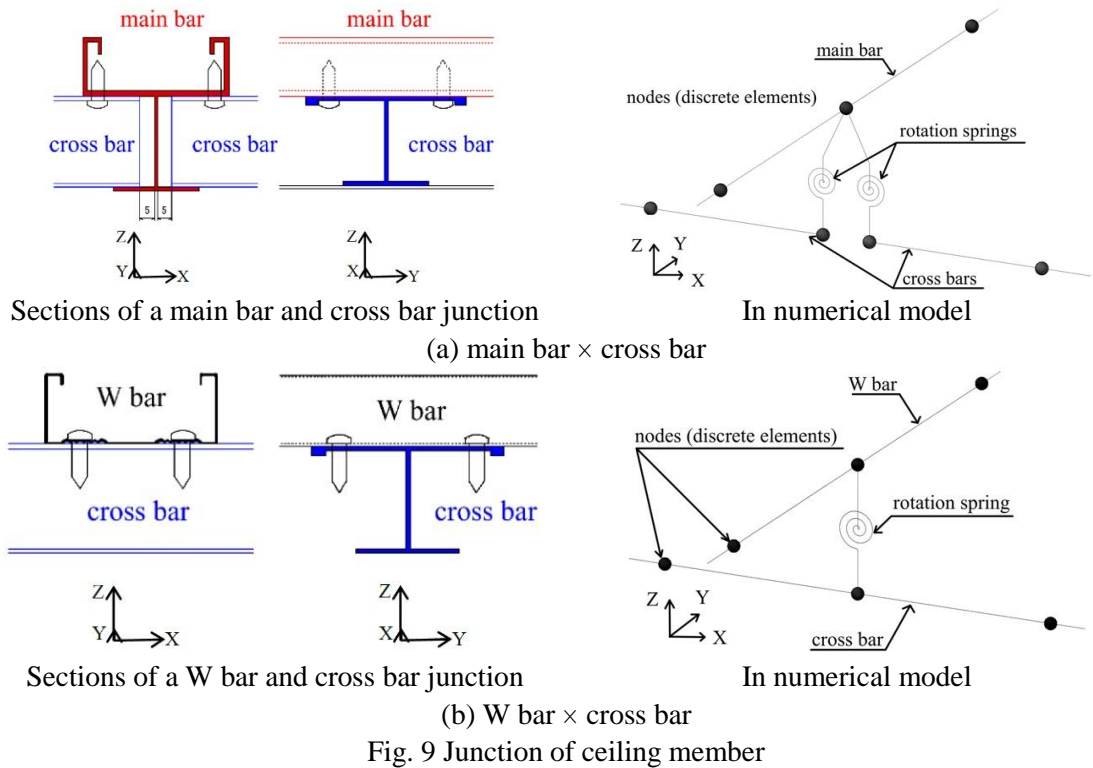Extruded aluminum profile. Molding is allocated around the periphery of the new seismic integrated ceiling.

Sections of a main bar and cross bar junction

In numerical model

(a) main bar × cross bar

Sections of a W bar and cross bar junction

In numerical model

(b) W bar × cross bar

Fig. 9 Junction of ceiling member
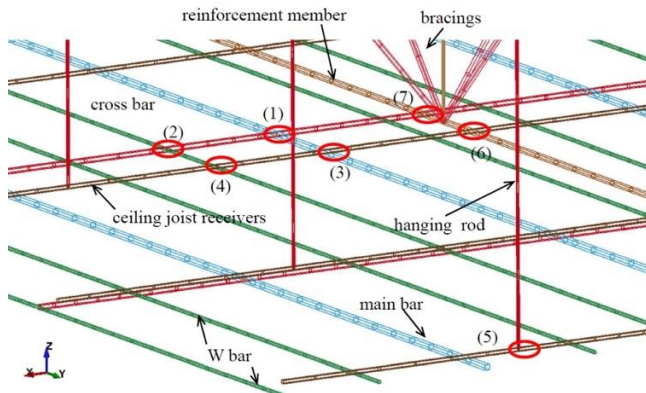
** glass wool panels
Finishing material which are allocated in the grid which comprised of main bars and cross bars.

2.2 Overview of numerical model

Fig. 5 depicts the overview (top, front and side) of the numerical model, which is created by beam elements, which in turn comprise main bars, cross bars, W bars, ceiling joist receivers, reinforcement members (connected to vertical bracings), vertical bracings, and hanging rods. Considering the requirements of specific ceilings regarding the area of the ceiling surface (namely, the area of the ceiling surface should be over 200 m^2), deployment of the ceiling members, and analysis time, the numerical model is 18,310 mm long along the cross-bar direction (X direction) and 14,400 mm long along the main-bar direction (or the W-bar direction) (Y direction). The overall area of the ceiling surface is 263.664 m^2. The distance between the two adjacent main bars is 1,000 mm, while it is 1,500 mm between the two adjacent cross bars. The hanging length, which is the distance from the top of the hanging rods to the ceiling surface, is 1,500 mm. The distance between the two adjacent hanging rods is 1,200 mm along both the X and Y directions. The @ mark infers the installation interval of ceiling members.

2.3 Physical properties

Fig. 6 are cross sections of ceiling members used in the new seismic integrated ceilings and in

No.	Junction	Constraint conditions
(1)	A junction of main bar and cross bar	Rotation springs around Z axis
(2)	A junction of W bar and cross bar	
(3)	A junction of main bar and ceiling joist receiver	1. Translational displacement in Z direction is constrained
(4)	A junction of W bar and ceiling joist receiver	
(5)	A junction of hanging rod and ceiling joist receiver	2. Rotations around X-axis, Y-axis are same, respectively
(6)	A junction of ceiling joist receiver and reinforcement member	
(7)	A junction of cross bar and reinforcement member	Share the same translational displacement and rotations in all directions

Fig. 10 Constraint conditions

the numerical model. S-axis and t-axis are local coordinate system for ceiling members. The cross-sectional properties of each ceiling member are listed in Table 2. They are nominal values provided by the corresponding manufactures. Because of the lack of data, the second moments of area, Iss and Itt, of the main bars and cross bars are calculated according to the cross sections in Fig. 6. The cross-sectional area of the hanging rods is the effective cross-sectional area. Iss and Itt are the second moment of area around s-axis and t-axis (shown in Fig.3), respectively.

Table 3 lists the physical properties of each ceiling member. The mass-density, Young's modulus, Poisson's ratio, and Yield strength of each ceiling member are the standard values of the corresponding materials. The yield strength of the STKMR11A is assumed to be 203 N/mm^2, which is 70% of the tensile strength of STKMR11A stated in the JIS G 3445 (2016).

As shown in Fig. 7, main bars (or W bars) are connected with cross bars at the junctions via screws. Thus, the junctions of main bars × cross bars and W bars × cross bars are regarded as rotation springs because these junctions are structurally critical in the system. Their rigidities are defined in our previous studies (Lyu *et al*. 2019a). Fig. 8 shows the rigidities of the rotation springs; the rigidities are computed using the approaches proposed in our previous studies (Lyu *et al*. 2019a). The first break point of the rotation spring is determined by the moment at the equivalent allowable load, which is 2/3rd of the equivalent damaged load. Notably, the "damaged load" is calculated by using the methods stated in Notification no. 771, whether or not the damage occurs in reality.

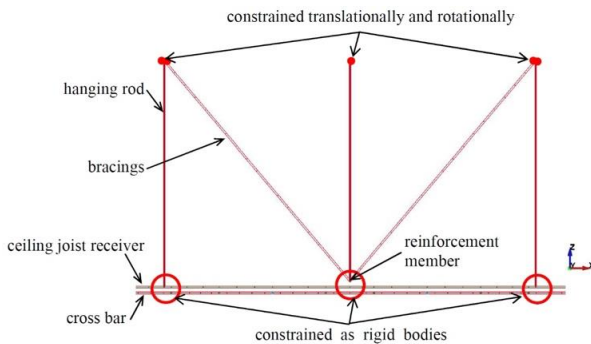Fig. 9 are the plan views of junctions of main bar (or W bar) and cross bar (see also Fig. 3(1)-

Fig. 11 Details around bracings

3(2)); and the corresponding models in the numerical model. Black circles represent discrete node elements in the numerical model. Lines are only used to help understand the positional relations of ceiling members; these lines don't exist in the numerical model. As shown in Fig. 9(a), there are 2 cross bars and 1 main bar in each junction. Therefore, the number of the rotation springs in each junction of main bars × cross bars is set as 2. Of the junction of W bars ×cross bars, since there are only 1 cross bar and 1 W bar in each junction (Fig. 9(b)), the number of the rotation springs in each junction of main bars × cross bars is set as 1.

2.4 Constraint conditions

Figs. 10-11 are the constraint conditions of the numerical model. Main bars and W bars are connected to cross bars with rotation springs around Z axis; rigidities have been defined in Fig. 8. Nodes at each junction of ceiling joist receivers and main bars (or W bars) are set to share the same translational displacements in X, Y, and Z directions; rotations around the X axis and Y axis are same, respectively. All nodes of ceiling joist receivers are translationally constrained in the Z direction.

Nodes of the top of bracings and hanging rods are completely fixed translationally and rotationally. Junctions of bracings (or hanging rods) and other ceiling members are defined as rigid bodies.

2.5 Analysis conditions

Static and seismic-response analyses were conducted to evaluate the seismic performance of the new seismic integrated ceiling with large area, and they are discussed in Sections 3.1 and 4.1, respectively.

The damping ratio in this numerical model is assumed to be 1.0%. The damping ratio for the suspended ceilings has not been clarified. In general, as the damping ratio for the steel structures is considered to be 2.0%, the damping ratio is set to be 2.0% in some papers. But considering the safety issue, the damping ratio is assumed as a lower value of 2.0%, that is, 1.0% in this numerical model.

As the numerical model in this paper is created by the beam elements, the nonlinear source has not been taken into consideration. For the same reason, the torsional bulking is considered in the numerical model, while the local bulking is not.
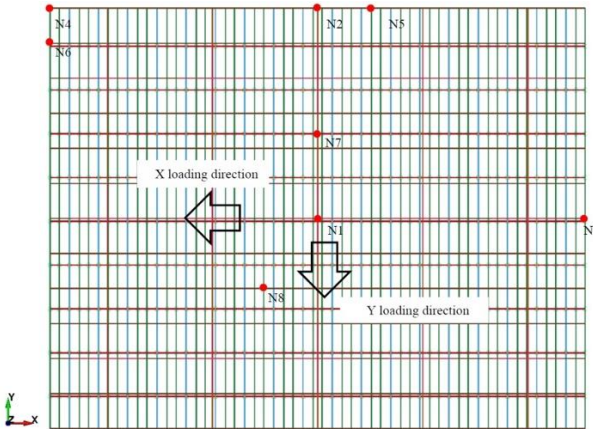
Fig. 12 Loading direction (static analysis)

3. Static analysis

3.1 Analysis conditions

To evaluate the seismic performance of the new seismic integrated ceilings in a large scale, horizontal forces ranging from 0 to 10.0 G were input along the X and Y directions during the static analysis. However, 2.2 G only is required in the Notification no. 771, which is assumed to be the horizontal inertial force in moderate earthquakes (occur once in every 50 years by definition). Fig. 12 shows the loading directions and the nodes to be evaluated. N1-N8 are nodes as follows:

N1:   The center of the main bar located on the center line, which is also the central of the ceiling.
N2:   One center of the ceiling joist receiver located at the edge of the ceiling.
N3:   One end of the ceiling joist receiver located in the center of the ceiling.
N4:   One of the edges of the ceiling in both X and Y direction.
N5:   One end of W bar located in the center of bracings.
N6:   One end of the ceiling joist receiver located on the edge of ceiling
N7:   The center between the two adjacent bracings on the reinforcing member.
N8:   One location in the square surrounded by the adjacent 4 sets of bracings.

3.2 Results of static analysis

Fig. 13 shows the relationship between the scale factor of gravitational acceleration *G* and the horizontal displacement of nodes along, respectively, the X and Y directions. The scale factor of *G* is obtained by dividing the input acceleration by the gravitational acceleration (i.e., 9806.65 mm/s^2). The direction of the horizontal displacement is the same as the loading direction.

In all the cases, the node in the center of the entire ceiling surface (N1) displaces only a little even under the force of 10.0 G (displacement of approximately 0.51 mm). Under the same acceleration, displacements increased as the nodes are away from the center of the ceiling surface. As far as the specified nodes are concerned, the ceiling surface is considered to displace in an elastic state before reaching approximately 5.0 G (i.e., N2 along the X direction and N6 along Y
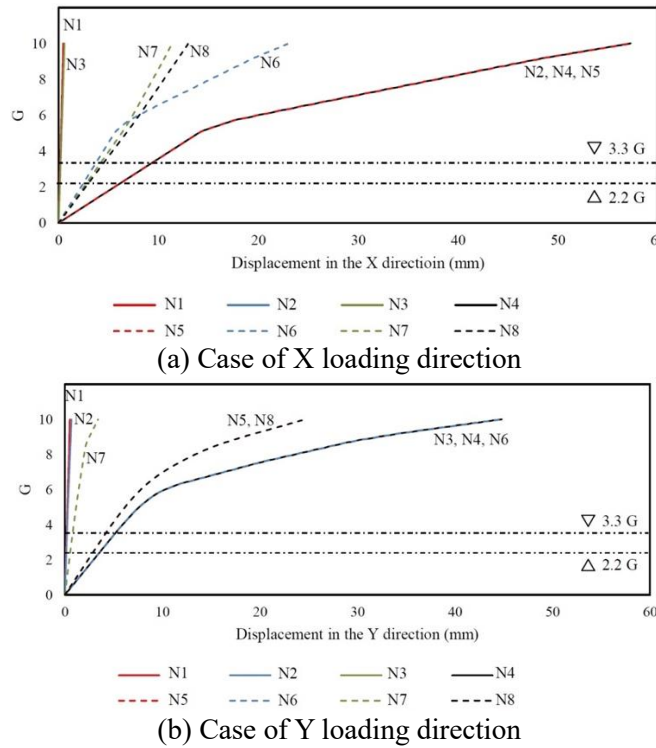
(a) Case of X loading direction

(b) Case of Y loading direction

Fig. 13 Relationship between the scale factors of gravity (*G*) and horizontal displacement of nodes

direction). This infers that the new seismic integrated ceiling can keep in elastic manner even when the horizontal inertial force is 5 times of its weight.

Furthermore, although some locations plasticized at some points, the maximum displacement in the case of X loading direction is about 57.31 mm, while about 44.80 mm in the case of Y loading direction by 10.0 G, which were all under 60 mm. Notably, 60 mm is also the minimum distance between the perimeter of the suspended ceiling and building components such as walls, columns, etc., as stated in Notification no. 771 (2013), whose technical standard stipulates that the calculation of this displacement for conventional suspended ceilings to be under the conditions of the horizontal seismic intensity 2.2 G and safety ratio 1.5. Because the screw joints and ceiling members were not damaged during the entire static analysis, the deformation of the ceiling members need not be discussed.

Figs. 14-17 are results of the static analysis. Figs. 14-15 depict the deformation of the numerical model under 3.3 G (in scale factor of 50) in the X and Y loading direction. Figs. 16-17 are the distribution of moment of forces on rotation springs, which are in accordance with Figs. 14-15, respectively. 3.3 G is 1.5 times of 2.2 G, which is considered to be the scale factor for great earthquakes. The horizontal and vertical axis of figures are X- and Y-coordinates of the numerical model. Bubbles in blue are positive moment of forces, while in white are negative. The size of bubbles is positively correlated to the moment of force. The maximum values (absolute value) are marked red.

It can be confirmed from these results that:
1) In the case of the X loading direction, moments of forces are same along with the X
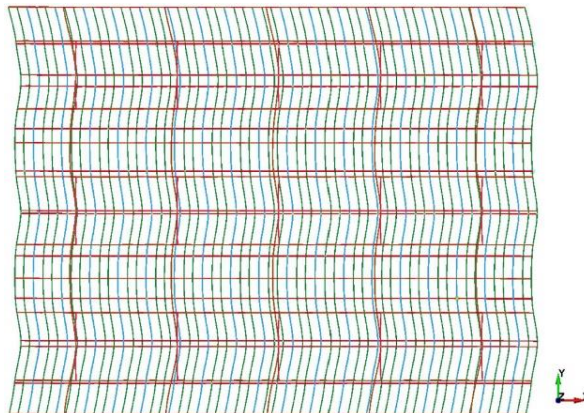
Fig. 14 Deformation of the numerical model under 3.3 G (X loading direction) (in scale factor of 50)
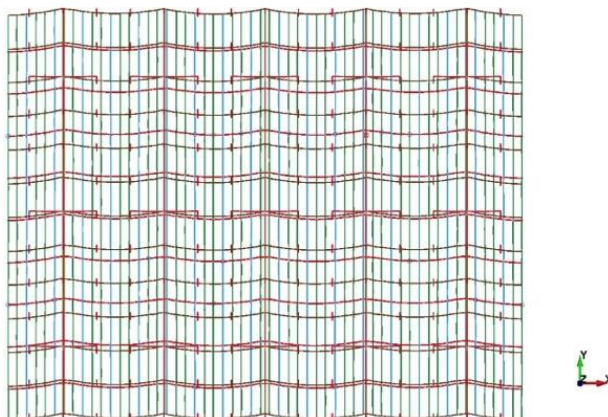

Fig. 15 Deformation of the numerical model under 3.3 G (Y loading direction) (in scale factor of 50)

direction but varies along with the Y direction (Fig. 16).

2) In the case of X loading direction, moments of forces on junctions in 2 cross bars that closed to the edge of ceiling surface are large while small along with the cross bar near the center of the ceiling surface (Fig. 16); this is because the two edges of main bars and cross bars (from the edge to the first hanging rod) can be regarded as cantilevers, which the largest moment of forces are larger around the constraint points.

3) In the case of the Y loading direction, moments of forces are same along with the Y direction but varies along with the X direction (Fig. 17).

4) In the case of the Y loading direction, moments of forces vary with a certain rule (Fig. 17). Moment of forces around the reinforcement members are higher than that apart from the reinforcement members. This is because reinforcement members are also acted to resist forces during

the case of Y loading direction and hence resulted in eccentricity around the reinforcement.

5) Analysis results 1) and 2), and 3) and 4) are consistent with Fig. 13 and Fig. 15, respectively.
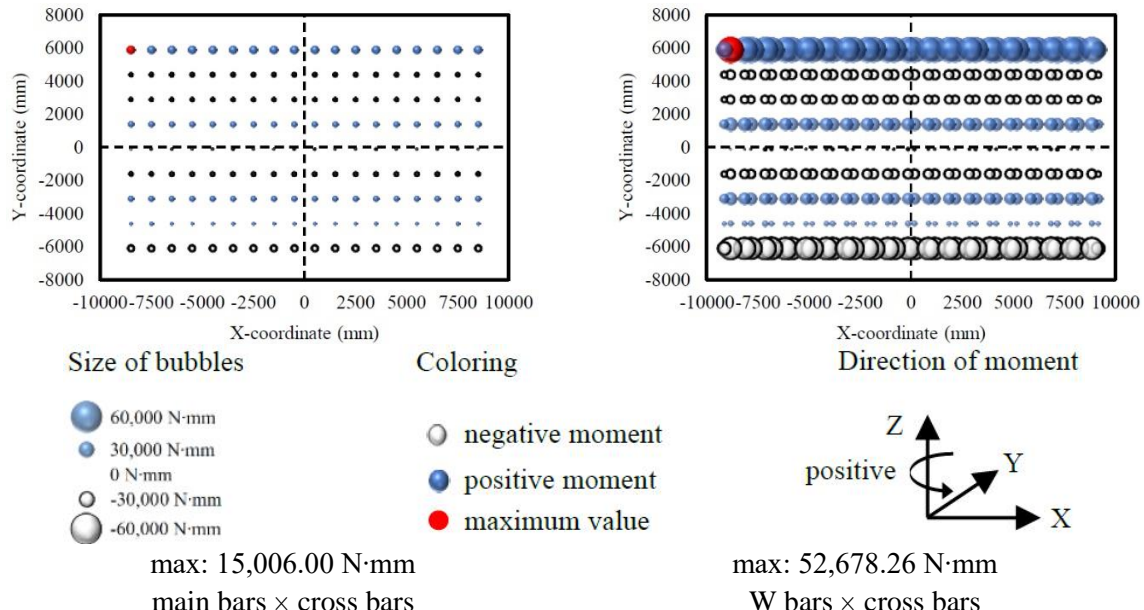
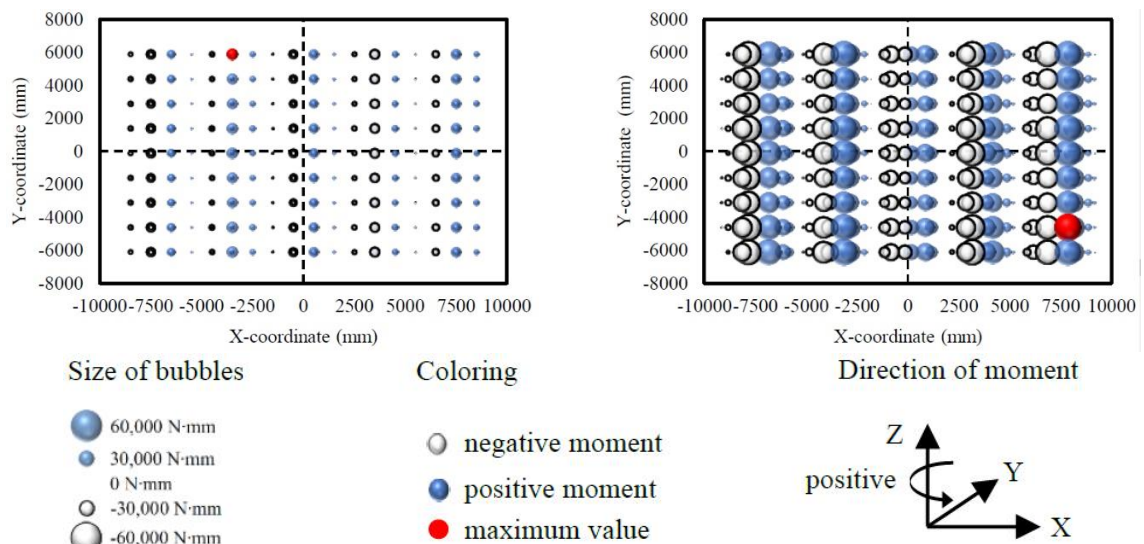Fig. 16 Distribution of moments on the rotation springs (X loading direction)

max: 15,006.00 N·mm
main bars × cross bars

max: 52,678.26 N·mm
W bars × cross bars

Fig. 17 Distribution of moments on rotation springs (Y loading direction)

max: 22,321.45 N·mm
main bars × cross bars

max: 54,495.08 N·mm
W bars × cross bars

In all the cases, along both the loading directions, i.e., the X and Y directions, the moments of forces on all the rotation springs at the junctions of the main bars and W bars and the cross bars are lower than the equivalent allowable moment (i.e., 3.0×10^4 N·mm for main bars × cross bars, and 6.0×10^4 N·mm for W bars × cross bars (Lyu *et al.*, 2019a)).
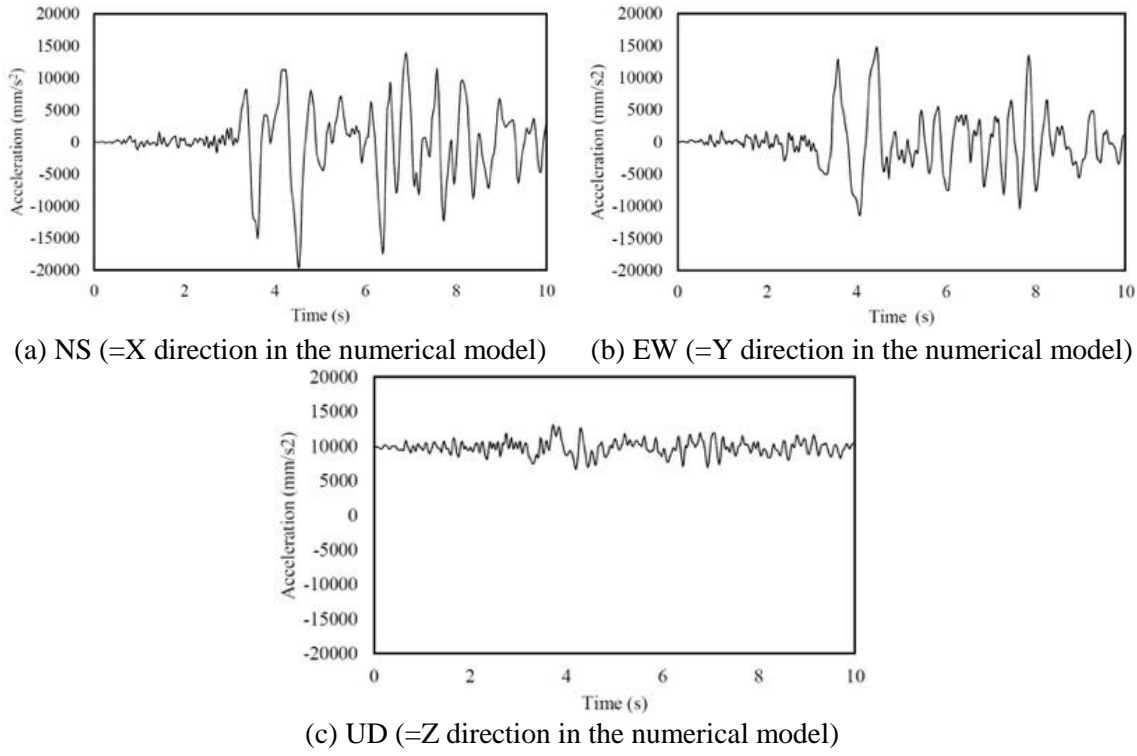
(a) NS (=X direction in the numerical model)   (b) EW (=Y direction in the numerical model)

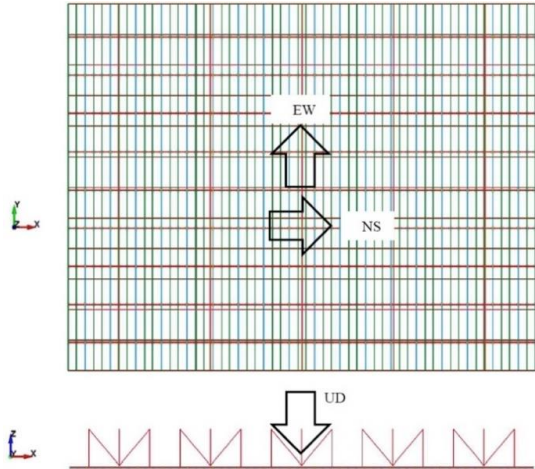(c) UD (=Z direction in the numerical model)

Fig. 18 Input acceleration

Fig. 19 Loading direction (seismic response analysis)

4. Example of seismic-response analysis

4.1 Analysis conditions of seismic response analysis

The seismic performance is evaluated by the static analysis discussed in Section 3. In this

X direction   Y direction

(a) N1

X direction   Y direction

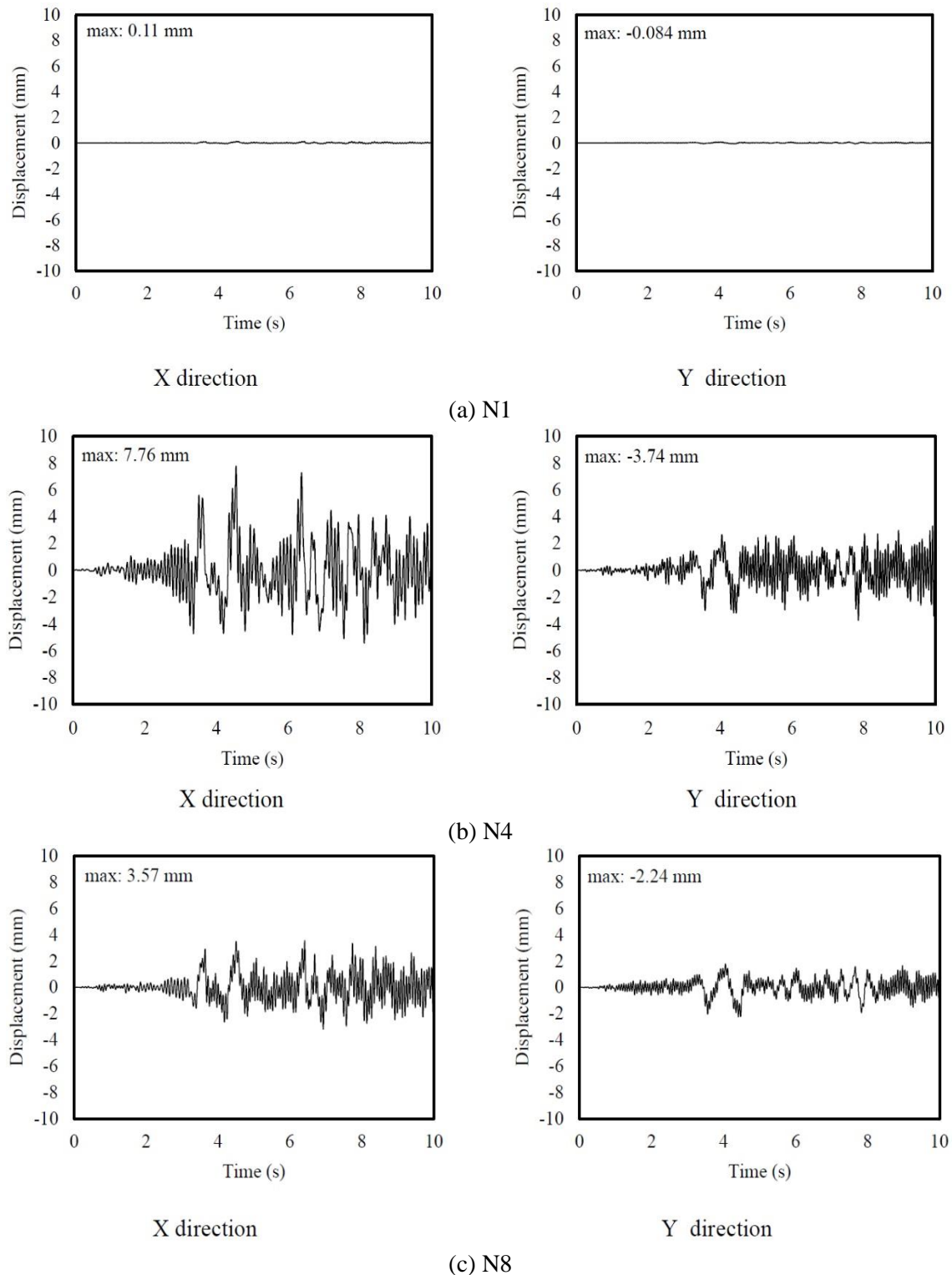(b) N4

X direction   Y direction

(c) N8

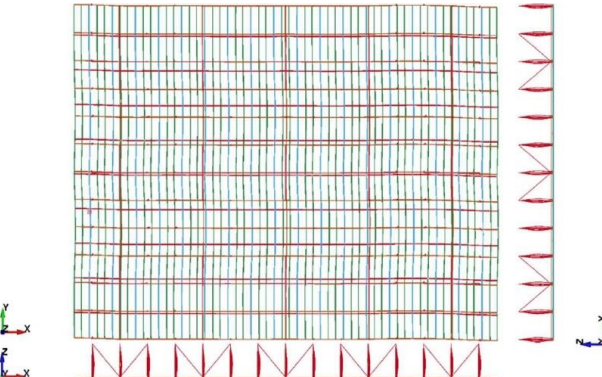Fig. 21 Displacement response time history

Fig. 22 Deformation of the numerical model (when the maximum of horizontal displacement appears)

section, the recorded earthquake waves will be input as loading to confirm the behaviors of the new seismic integrated ceiling during 3-dimensional earthquakes. In this study, JMA Kobe earthquake waves (maximum acceleration: 818 cm/s^2 (= 0.83 G, NS direction)), which recorded by the Japan Meteorological Agency during the 1995 Hyogo-ken Nanbu earthquake, were used as an example.

Figs. 18(a)-18(c) depict the input acceleration. The horizontal acceleration is amplified to approximately 2.0 G by multiple 2.4 from the original waves uniformly. In actual cases, the acceleration will be amplified due to this process in which the earthquake waves transfer from the ground to the buildings and then to the suspended ceilings. In this paper, the amplification rate is assumed to be 2.4. The terms NS, EW, and UD stand for the north-south, east-west, and up-down directions, which correspond to the X-, Y-, and Z direction in the numerical model, respectively (see Fig. 19). Because suspended ceilings are affected by the gravity along the Z direction, the gravitational acceleration was considered (original data + 9806.65 mm/s^2). To reduce the calculation time and enhance the efficiency and effectiveness of the numerical model, the earthquake waves in the duration from 29 s to 39 s of the total duration, when the vibration was detected by the seismometer, were selected as the input earthquake waves.

4.2 Results of seismic response analysis

Fig. 20 compares the time history of the acceleration response of nodes N1, N4, N8 (see Fig. 12). The time interval of the input acceleration is 0.02 s. The maximum acceleration during the entire loading period was 24108.19 mm/s^2, which occurred in N4 along the Y direction. Fig. 21 shows the time history of the displacement response for N1, N4, and N8. The maximum horizontal displacement was approximately 7.76 mm, which occurred in N4 along the X direction. As confirmed in the static analysis, the center of the ceiling surface (N1) merely vibrated during the whole loading period. The perimeter of the whole ceiling surface (N4) vibrated violently more than other locations of ceiling surface. The center of the square surrounded by the adjacent 4 sets of vertical bracings, i.e., N8, shows the similar behavior as N4, but the value is limited to a smaller range than N4.
Fig. 22 depicts the deformation of the numerical model at the time of 4.54 s, when the max translational displacement occurs (Fig. 21(b)), in the scale factor of 50. Fig. 23 shows the
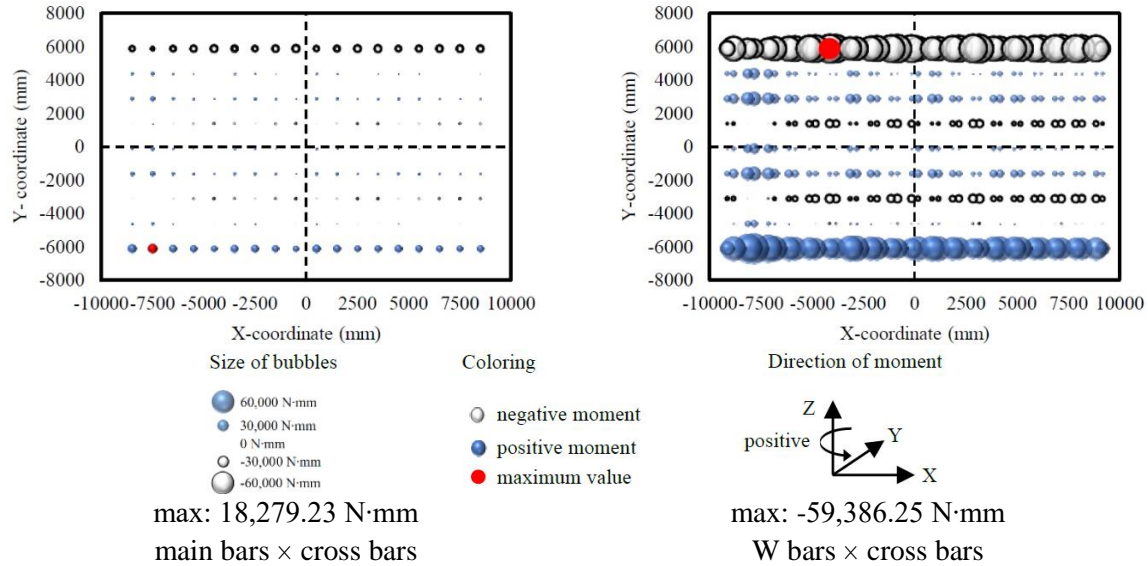
Size of bubbles

60,000 N·mm
30,000 N·mm
0 N·mm
-30,000 N·mm
-60,000 N·mm

Coloring

○ negative moment
● positive moment
● maximum value

Direction of moment

positive

max: 18,279.23 N·mm   max: -59,386.25 N·mm

main bars × cross bars   W bars × cross bars

Fig. 23 Distribution of moments on rotation springs (when the maximum horizontal displacement appears)

Size of bubbles

60,000 N·mm
30,000 N·mm
0 N·mm
-30,000 N·mm
-60,000 N·mm

Coloring

○ negative moment
● positive moment
● maximum value

Direction of moment

positive

max: -16,750.92 N·mm   max: -46,303.20 N·mm

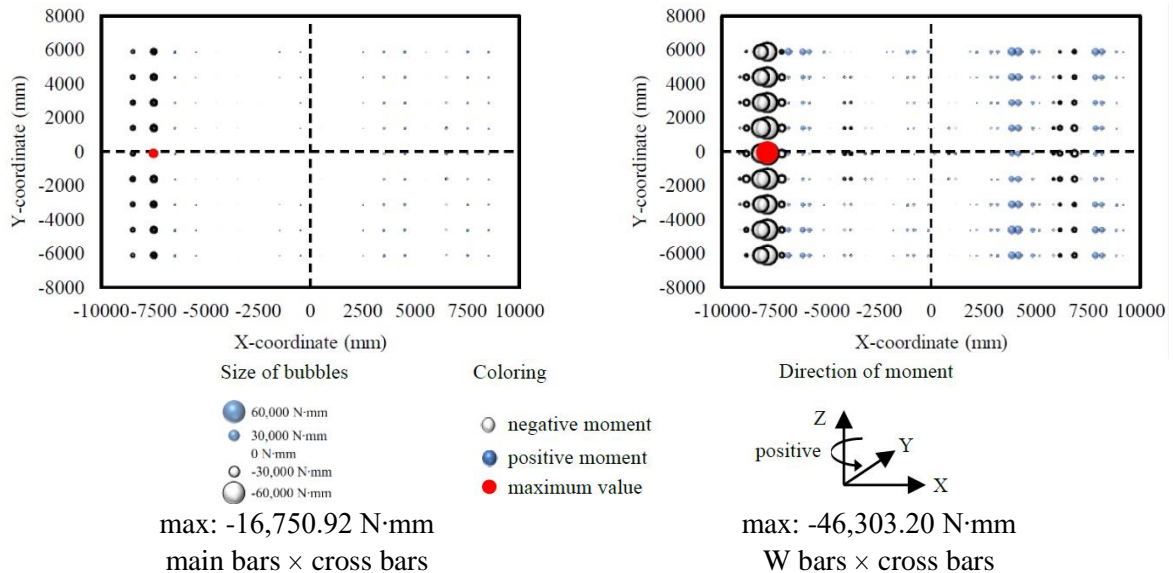main bars × cross bars   W bars × cross bars

Fig. 24 Distribution of moments on rotation springs (when the maximum acceleration appears) of moments on rotation springs (when the maximum horizontal displacement appears)

distribution of moments forces of all the rotation springs at the time of 4.54 s, while Fig. 24 shows the distribution of moment forces of all the rotation springs when the max acceleration occurs (Fig. 21(b)). Fig. 23 shows a similar behavior as confirmed in the static analysis (case of the X loading direction), but the moments of forces on the edge of the ceiling surface are greater than those in the static analysis, proving that stresses concentrated more than during the static analysis. Fig. 24

shows that stresses may concentrate on certain parts of ceiling members at some time during earthquakes. This phenomenon is greatly different from the static analysis.

5. Conclusions

In this paper, numerical models for a new seismic integrated ceiling with an area of approximately 264 m^2 were proposed and discussed. Additionally, the seismic performance of the ceiling was evaluated via static analysis using LS-DYNA. The seismic behaviors of this ceiling model under 3-dimensional earthquake waves were shown. In the static analysis, forces ranging from 0 to 10.0 G were loaded along the X- and Y direction, respectively. In the seismic-response analysis, JMA Kobe earthquake waves were used as a seismic load. Static analysis was used to evaluate the seismic performance. The distribution of the moments of forces on all the rotation springs (i.e., screw joints between main bars (or W bars) and cross bars) were quantified. It indicates that the new seismic integrated ceilings can be installed with the space between the ceiling surface and peripheral walls or other structural components within 60 mm. Via the seismic-response analysis, the maximum acceleration and maximum horizontal displacement of the new seismic integrated ceiling were quantified. Via the seismic-response analysis, it shows the fact that the new seismic integrated ceilings during earthquakes can perform as similar as during the static analysis (or static tests), but may also perform greatly different from that during the static analysis (or static tests). It implies the essentiality of the seismic-response analysis on the safety check during the research and development of the suspended ceilings.

Evaluating the seismic performance under earthquake waves with different predominant periods, effect of openings and the corresponding reinforcement, effects of burden area of bracings, etc. are considered challenges for future studies.

Acknowledgments

References

Architectural Institute of Japan (2012), *Preliminary Reconnaissance Report of the 2011 Tohoku-Chiho Taiheiyo-Oki Earthquake*, Springer, Berlin, Germany.

Fiorino, L., Bucciero, B. and Landolfo, R. (2019), "Evaluation of seismic dynamic behaviour of drywall partitions, façades and ceilings through shake table testing", *Eng. Struct.*, **180**, 103-123. https://doi.org/10.1016/j.engstruct.2018.11.028.

Gilani, A.S.J., Takhirov, S.M. and Straight, Y. (2017), "Evaluation of seismic performance of suspended ceiling systems using dynamic testing and finite element analysis", *16th World Conference on Earthquake Engineering*, Santiago, Chile, January.

Instruction of Housing Bureau of Ministry of Land, Infrastructure, Transport and Tourism, No. 357 (2001),

Ministry of Land, Infrastructure, Transport and Tourism.

Isobe, D., Fujiwara, T., Yamashita, T., Tagawa, H. and Sasaki, T. (2017), "Collapse simulation of wide-area suspended ceiling system using finite element method", *J. Struct. Constr. Eng., AIJ*, **82**(741), 1727-1736. https://doi.org/10.3130/aijs.82.1727

Kambe, H., Ishihara, T., Yamashita, K., Suzuki, K. and Nagano, M. (2017), "Static loading tests on in-plane shear behavior of grid-type system ceilings and evaluation of their seismic responses", *AIJ J. Technol. Des.*, **23**(55), 839-843. https://doi.org/10.3130/aijt.23.839

Lu, Y., Mosqueda, G., Han, Q.H. and Zhao, Y.F. (2018), "Shaking table tests examining seismic response of suspended ceilings attached to large-span spatial structures", *J. Struct. Eng. (United States)*, **144**(9). https://doi.org/10.1061/(ASCE)ST.1943-541X.0002140.

Lyu, Z.L., Sakaguchi, M., Saruwatari, T. and Nagano, Y. (2019), "Tests of systematized ceilings and the construction of simulation models", *Advan. Comput. Design.*, **4**(4), 381-395. http://dx.doi.org/10.12989/acd.2019.4.4.381

Mizushima, Y., Mukai, Y., Namba, H., Taga, K. and Saruwatari, T. (2018), "Super-detailed FEM simulations for full-scale steel structure with fatal rupture at joints between members-Shaking-table test of full-scale steel frame structure to estimate influence of cumulative damage by multiple strong motion: Part 1", *Japan Architect. Rev.*, **1**(1), 96-108. http://dx.doi.org/10.3130/aijs.81.61.

Notification No. 771 (2013), Ministry of Land, Infrastructure, Transport and Tourism. [Japanese]

Pourali, A., Dhakal, R., Tasligedik, A.S. and Macrae, G. (2018), "Experiments on seismic compatibility of low-damage drywall partitions and suspended ceilings", *11th US National Conference on Earthquake Engineering (11NCEE)*, Los Angeles, USA, June.

Qi, L.J., Kunitomo, K., Kurata, M. and Ikeda, Y. (2020), "Investigating the vibration properties of systematized ceiling systems considering interactions with surrounding equipment", *Earthq. Eng. Struct. Dyn.*, **49**(3). https://doi.org/10.1002/eqe.3264.

Ryu, K.P. and Reinhorn, A. (2017), "Experimental study of large area suspended ceilings", *J. Earthq. Eng.*, **23**(6), 1001-1032. https://doi.org/10.1080/13632469.2017.1342294

Sasaki, T., Aoi, A., Kajiwara, K., Tagawa, H. and Sato, D. (2017), "Collapse mechanism of wide-area suspended ceiling based on full-scale shake table experiment of school gymnasium", *16th World Conference on Earthquake Engineering*, Santiago, Chile, January.

Soroushian, S., Rahmanishamsi, E., Jenkins, C. and Maragakis, E. (2019). "Fragility analysis of suspended ceiling systems in a full-scale experiment", *J. St. Eng. (United States)*, **145**(4), https://doi.org/10.1061/(ASCE)ST.1943-541X.0002273.

Ushio, Y., Saruwatari, T. and Nagano, Y. (2019), "A new design method for site-joints of the tower crane mast by non-linear FEM analysis," *Advan. Comput. Design*, **4**(4), 343-365. http://dx.doi.org/10.12989/acd.2019.4.4.343

TK